ISSN 0016-7932, Geomagnetism and Aeronomy, 2022, Vol. 62, No. 4, pp. 388–398. © Pleiades Publishing, Ltd., 2022, corrected publication 2022.
Russian Text © The Author(s), 2022, published in Geomagnetizm i Aeronomiya, 2022, Vol. 62, No. 4, pp. 470–481.

Geomagnetic Storm Prediction Based on the Neural Network Digital Processing of Joint Observations of the URAGAN Muon Hodoscope and Neutron Monitor Stations

V. G. Getmanov[a, b, *], V. E. Chinkin[a, **], R. V. Sidorov[a, *], A. D. Gvishiani[a, b, ****], M. N. Dobrovol'skii[a, *****], A. A. Soloviev[a, b, ******], A. N. Dmitrieva[a, c, *******], A. A. Kovylyaeva[a, c, ********], and I. I. Yashin[a, c, *********]**

[a] *Geophysical Center, Russian Academy of Sciences, Moscow, Russia*
[b] *Institute of Physics of the Earth, Russian Academy of Sciences, Moscow, Russia*
[c] *National Research Nuclear University, Moscow, Russia*
**e-mail: vgetm2015@yandex.ru*
***e-mail: v.chinkin@gcras.ru*
****e-mail: r.sidorov@gcras.ru*
*****e-mail: adg@wdcb.ru*
******e-mail: m.dobrovolsky@gcras.ru*
*******e-mail: a.soloviev@gcras.ru*
********e-mail: ANDmitriyeva@mephi.ru*
*********e-mail: AAKovylyaeva@mephi.ru*
**********e-mail: IIYashin@mephi.ru*

Received October 13, 2021; revised January 21, 2022; accepted March 30, 2022

Abstract—A method for predicting geomagnetic storms based on the neural network digital processing of joint observations of the URAGAN muon hodoscope and the international system of neutron monitor stations has been proposed. A time series of *Dst* indices are used. Formulas for extrapolating model estimates of *Dst* indices have been developed. A fully-connected feed-forward neural network has been used. Prediction decision rule has been implemented. The probability characteristics of geomagnetic storm prediction have been estimated. An experimental study of the prediction method confirmed its effectiveness. It has been shown that the observations of the hodoscope–monitor system increased the probability of correctly predicting geomagnetic storms compared to using each of the observations separately.

DOI: 10.1134/S0016793222040089

1. INTRODUCTION

Geomagnetic disturbances usually occur during extreme events in the heliosphere, which are the consequence of plasma formations in the form of solar coronal mass ejections (CMEs). Geomagnetic storms (GMS's) are geomagnetic disturbances with an amplitude greater than a given one. GMS prediction is an urgent scientific problem, which to date has not been exhaustively solved.

Geomagnetic activity is characterized by various geomagnetic indices, among which the *k*-, *kp*-, and *ap*-indices are quite common (Menvielle et al., 2011). This article is based on *Dst* indices, which are frequently used in geomagnetism practice (Sugiura and Kamei, 1991). These indices are measured in nT and are determined by hourly averaging of the values of the meridional geomagnetic field components for magnetic observatories located at the Earth's equator. For quiet states of the magnetosphere, *Dst* indices are mainly in the range −50...+20 nT; for GMS, *Dst* indices are in the range −150...−50 nT, and, in exceptional cases, they are outside this range.

This article uses information from the following sources:

1. Time series of matrix observations from the database (Real-time URAGAN, 2015) of the URAGAN Muon Hodoscope (MH) constructed at the MEPhI (Yashin et al., 2015). Here, we consider one possible simplification of the GMS prediction problem: the time series of matrix observations of the MH is converted into a scalar time series obtained by averaging the MH observation matrices. This time series is formed by the MH-observations proportional to the intensity of the muon fluxes detected by the URA-

GAN hodoscope. Matrix time series of MH-observations for GMS prediction will be the subject of research in the following publications.

2. Time series of scalar observations of the worldwide network of neutron monitors (NMs) (NMDB, 2021). The functions of the isotropic components of the NM observations derived from the global survey method are used here (Abunina et al., 2018). This time series is formed by the values of NM observations proportional to the intensity of neutron fluxes detected by neutron monitors.

3. Time series of scalar *Dst* indices at the website of the World Data Center of Geomagnetism (WDCG), Kyoto (World Data Center, 2021).

GMS predictions are determined by the type of used information sources, hardware, mathematical methods, and variants of the implemented applied problems. There are a number of services of different departmental and state affiliation that publish information on GMS predictions.

For the Russian Federation, the IZMIRAN's Space Weather Prediction Center (Gaidash et al., 2016; Prediction Center, 2016; Gaidash et al., 2017) should be noted, which offers more than 20 types of products related to space weather and GMS prediction to consumers, including a 3-day forecast of 3-hour *k*- and *kp*-indices, an 8-day geomagnetic forecast based on average daily *ap*-indices and probabilities of the highest *kp*-indices per day, geomagnetic activity forecasts based on *ap*-indices for 55 days, etc.

The activity of the Laboratory of X-ray Astronomy of the Physical Institute in solving the problem of GMS prediction using solar radiography technologies should be noted. The website (Laboratory of X-ray, 2017) provides calculations of *kp*-indices for 3- and 27-day prediction intervals, which are carried out taking into account estimates of solar wind parameters.

It is necessary to mention the Space Weather Prediction Center of the National Oceanic and Atmospheric Administration (NOAA, United States) (NOAA/NWS, 2021), which deals with variants of GMS predictions. The NOAA website publishes data on *kp*- and *ap*-indices for 1–4-week prediction intervals. Images from the Extreme ultraviolet Imaging Telescope (EIT) and the Large Angle and Spectrometric Coronagraph (LASCO) (NOAA/NWS, 2021) are used for the GMS predictions in order to estimate solar corona heating characteristics and CME processes and to determine corona effect on the solar wind. LASCO images are used for the WSA-Enlil prediction model (NOAA/NWS, 2021), which has been in operation since 2011. This large-scale physical model of the heliosphere is designed to provide 1–4-day advance warning of changes in solar wind structures and CME motion directions. The Advanced Composition Explorer (ASE, United States) spacecraft (NOAA/NWS, 2021) launched in 1997 is used, which is permanently located at the Lagrange point at a distance of 1.44 million km from Earth on a straight line connecting the Earth and the Sun. This spacecraft, which can be taken as a patrol satellite, continuously records parameters of the solar wind and the interplanetary magnetic field and automatically transmits them to the Earth; the recorded parameters are published on the NOAA websites for further processing.

GMS prediction can be implemented on the basis of a number of methods, e.g., using probabilistic models or recognizing anomalies in time series. Thus, in (Dobrovol'skii et al., 2019; Chinkin et al., 2019), the use of special 2D variation functions of muon fluxes and indicator matrices was proposed for matrix MH observations.

Neural networks (NN) are widely used in solar-terrestrial physics in the problems of predicting (recognizing) extreme events in the heliosphere and magnetosphere (Barkhatov and Revunov, 2010). A number of publications related to NNs, *Dst* indices, and GMS's differ in the variants of the used methods, software products, and information sources (databases). These circumstances introduce significant variation in the formulation of the problems.

In (Wu and Lundstedt, 1997; Stepanova and Pérez, 2000; Barkhatov et al., 2001; Dolenko et al., 2005; Pallocchia et al., 2006; Shirokii, 2015; Efitorov et al., 2018; Gruet et al., 2018) are materials concerning research into the GMS prediction using NN variants.

The aim of this article is to develop a GMS prediction method based on *Dst* index models, the combined use of MH and NM observations, extrapolation technology, and NNs. The proposed formulation in some details can be considered additional to the listed publications. The results obtained in the article on GMS prediction based on NN model estimates of *Dst* indices with extrapolation are intended for a number of scientific and technical applications, e.g., in case of possible sudden absence (omission) of *Dst* indices, GMS prediction can be implemented based on prebuilt models of *Dst* indices working only on MH and NM observations. The proposed GMS prediction can prove to be an alternative in case of possible patrol satellite failures.

2. ANALYSIS OF *Dst* INDICES AND MH, NM OBSERVATIONS

All variables used for NNs in this article were synchronized and sampled in hourly steps on a single UTC time scale. The time index k defined the sample points Tk, $T = 1$ h. The *Dst* indices $Y_D(k)$ and NM observations $Y_N(k)$ were implemented on the time interval January 1, 2002–December 31, 2018, and the MH observations $Y_M(k)$, in the interval January 1, 2008–December 31, 2018. Initial and final indices for Y_D took values $k_0 = 1$, $k_f = 149016$, for Y_M, indices $k_{01} = 52285$, $k_f = 149016$, and for $Y_N - k_{02} = 1$, $k_f = 149016$.

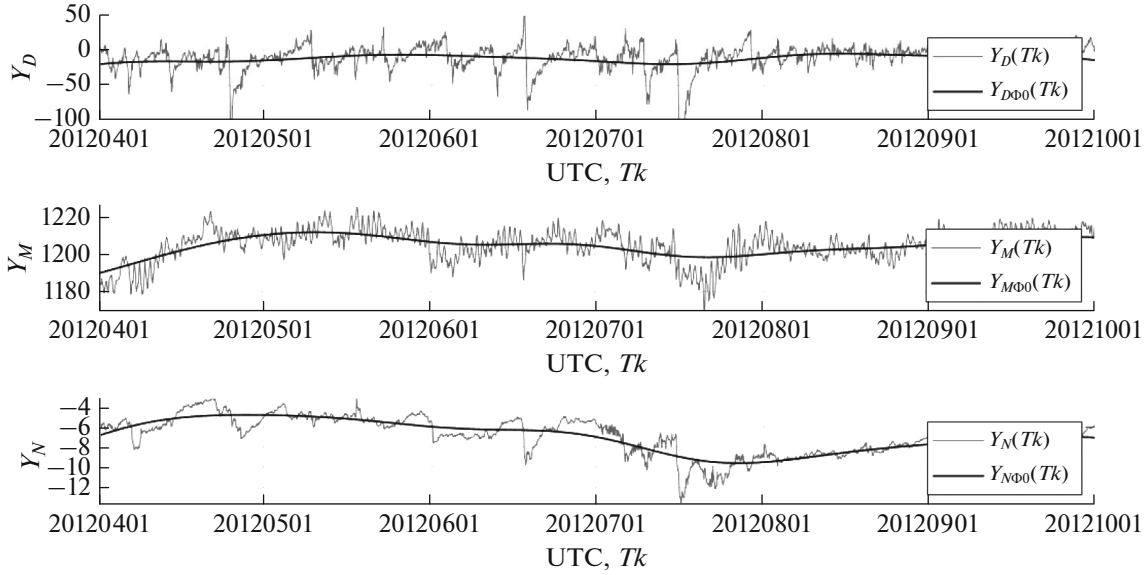

Fig. 1. Graphs of fragments of the initial MH and NM observations $Y_M(k)$, $Y_N(k)$, and *Dst* indices $Y_D(k)$.

Figure 1 contains examples of the plots of fragments of the initial variables $Y_D = Y_D(k)$, $Y_M = Y_M(k)$, and $Y_N = Y_N(k)$ for the 6-month time interval (April 1, 2012–September 30, 2012) as a function of time *Tk*. GMS events were determined by the inequality $Y_D(k) \le Y_{D0}$. For the threshold $Y_{D0} = -50$ nT, nine GMS events occurred in this interval. The analysis of $Y_D(k)$ in Fig. 1 led us to conclude that the average duration of GMS was on the order of 2–2.5 days. The consideration of the initial variables made it possible to conclude that for them the average period of additive uninformative low-frequency trends to be filtered was about 60–75 days. In Fig. 1, the uninformative trends $Y_{D\Phi 0}(k)$, $Y_{M\Phi 0}(k)$, and $Y_{N\Phi 0}(k)$ are shown as smooth lines.

We can see from the graphs that variables $Y_D(k)$ and $Y_N(k)$ can be represented as a sum of informative low-frequency trends and high-frequency noise. The variable $Y_M(k)$ can be represented as a sum of the informative low-frequency trend, interference components from daily fluctuations and high-frequency noise. The analysis of changes in informative low-frequency trends of the variables $Y_M(k)$, $Y_N(k)$ allowed us to conclude that these, in some cases, behave almost identically in time.

3. FORMULATION OF THE GEOMAGNETIC PREDICTION PROBLEM

In the practice of analyzing geomagnetic observations, it is sometimes customary to make a conclusion about the GMS prediction based on criteria that are formed on the basis of different variants of geomagnetic indices. A criterion based on comparing *Dst* indices with a given threshold is quite common and, to a certain extent, reliable in GMS prediction. However, sometimes the direct use of *Dst* indices for prediction can be problematic due to the fact that there can be none of them at the current and subsequent points in time, for various reasons.

There is a well-defined functional relationship between the *Dst* indices and the values of MH, MN observations that can be represented by a model scheme based on (Borog, 2008). The *Dst* index functions act as GMS indicators and their values are determined by the intensity of the interaction of the CME formations with the Earth's magnetosphere. The travel time of CMEs from the Sun to the Earth and the time of the start of the GMS, if it is counted from the time of emission of CMEs, is usually 1.5–2 days. Simultaneously, CMEs modulate intensities of relativistic proton fluxes approaching the Earth; their travel time from the Sun to the Earth is about 8 min. Proton fluxes enter into nuclear reactions with atoms of substances of the upper atmosphere, as a result of these reactions, muon and neutron fluxes are formed, the intensity of which is detected by the URAGAN hodoscope and neutron monitors. Modulations of proton flux intensities under certain conditions cause modulations of intensities of generated muon and neutron fluxes, i.e., values of MH, MN observations. The modulations of muon and neutron fluxes occur significantly earlier than the GMS; this fact is the basis for the proposed method for predicting GMS.

We will assume that:

— The current considered time is given, to which corresponds the time index k which satisfies the inequalities $k_{f0} + 1 \le k \le k_f$. The preceding times are those to which the time indices $k_{f0} + 1, \ldots, k - 1$ correspond, where k_{f0} is the given time index; the initial

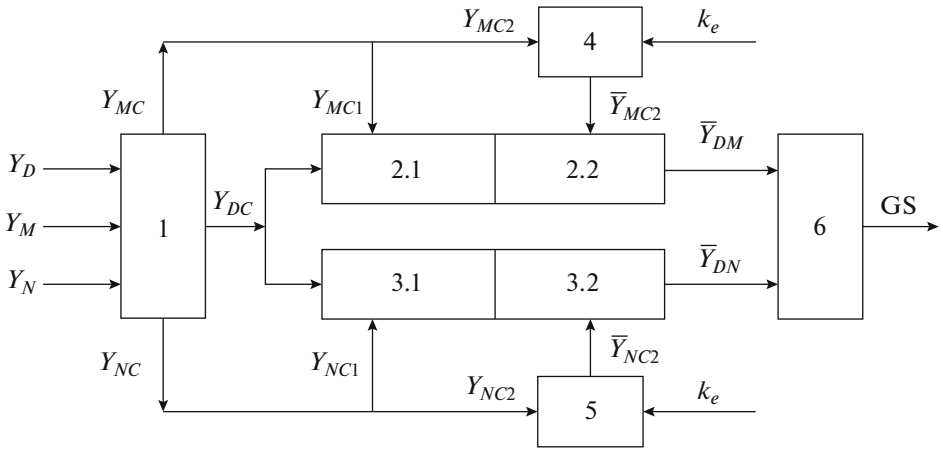

Fig. 2. A diagram of computational operations for solving the GMS prediction problem.

index k_0, the final index k_f, and the given index k_{f0} are related by the inequalities $k_0 < k_{f0} < k_f$.

— In the interval $k_{01} \le k \le k_{f0}$, a time series of MH observations and a time series of *Dst* indices are implemented; in the interval $k_{02} \le k \le k_{f0}$, a time series of NM observations and a time series of *Dst* index values.

— In the interval $k_{f0} + 1$, $k - 1$, k only the time series of MH and NM observations are implemented.

We will consider GMS prediction with respect to the current times with indices k on k_e indices forward.

The aim of the work is to create a system of model estimates of *Dst* indices in the interval $k_{f0} + 1 \le k \le k_f$ based on the implemented times series of *Dst* indices and MH, NM-observations in the intervals $k_{01} \le k \le k_{f0}$, $k_{02} \le k \le k_{f0}$ and use them for GMS prediction. For this problem, we apply a full-connected feed-forward NN and extrapolation technique in forming model estimates of *Dst* indices.

4. THE GENERAL PLAN FOR SOLVING THE GMS PREDICTION PROBLEM AND EXTRAPOLATION FORMULA

4.1. The general plan for solving the GMS prediction problem taking the formulation in item 3 of the formulation into account, is divided into five items, including

(1) algorithms for preliminary digital processing of initial *Dst* indices and MH, NM-observations in order to isolate significant informative components in them;

(2) algorithms for training and validation of NNs;

(3) algorithm for extrapolation of MH, NM-observations;

(4) a calculation-test algorithm for model estimates of *Dst* indices with NN-based extrapolation using extrapolated MH, NM-observations;

(5) a decision rule algorithm for GMS prediction.

Figure 2 presents a diagram of computational operations that explains the solution to the GMS prediction problem. The computational operations are subdivided into digital preprocessing block ***1***, blocks ***2.1, 3.1*** of MH, NM NN training, extrapolation blocks ***4, 5***, blocks ***2.2, 3.2*** for computing model estimates of *Dst* indices for MH, NM, and block ***6*** for decision making for GMS prediction.

Digital preprocessing algorithms for the initial *Dst* indices $Y_D = Y_D(k)$ and MH, NM observations $Y_M = Y_M(k)$, $Y_N = Y_N(k)$ implement their filtering (Filter Design, 2021) in order to remove high frequency noise and daily variations as well as to remove low-frequency uninformative trends and scale in order to ensure commensurability of the initial variables, which is necessary for efficient NN operation.

The results of the digital preprocessing are denoted as $Y_{DC} = Y_{DC}(k)$, $Y_{MC} = Y_{MC}(k)$, and $Y_{NC} = Y_{NC}(k)$. The scaling operation brings the preprocessing results to a single range: $Y_{\min} \le Y_{MC}(k) \le Y_{\max}$, $Y_{\min} \le Y_{NC}(k) \le Y_{\max}$, $Y_{\min} \le Y_{DC}(k) \le Y_{\max}$, $Y_{\min} = 0.7$, $Y_{\max} = 1.3$. Figure 3 shows example graphs of fragments of the variables $Y_{MC} = Y_{MC}(k)$, $Y_{NC} = Y_{NC}(k)$, and $Y_{DC} = Y_{DC}(k)$ obtained from the numerical preprocessing on the monthly time interval April 1, 2012–April 30, 2012.

The NN training stage for MH variables $Y_{MC1}(k)$ is implemented in the interval with indices $k_{01} + dk_{01} + 1 \le k \le k_{f0}$, for NM variables $Y_{NC1}(k)$, on indices $k_{02} + dk_{02} + 1 \le k \le k_{f0}$, variables $Y_{DC}(k)$ are implemented in these intervals. The values of dk_{01}, dk_{02} are set. The sequences of Δk-dimension vectors moving in unit steps and formed by these variables are fed to the NN input. The validation stage of NN models after training is performed for the indices $k_{01} \le k \le k_{01} + dk_{01}$ for MH variables and for the indices $k_{02} \le k \le k_{02} + dk_{02}$ for NM variables. As a result of the training and validation stages, MH, NM NN models for *Dst* indices are created. The testing stage is dedicated to computing

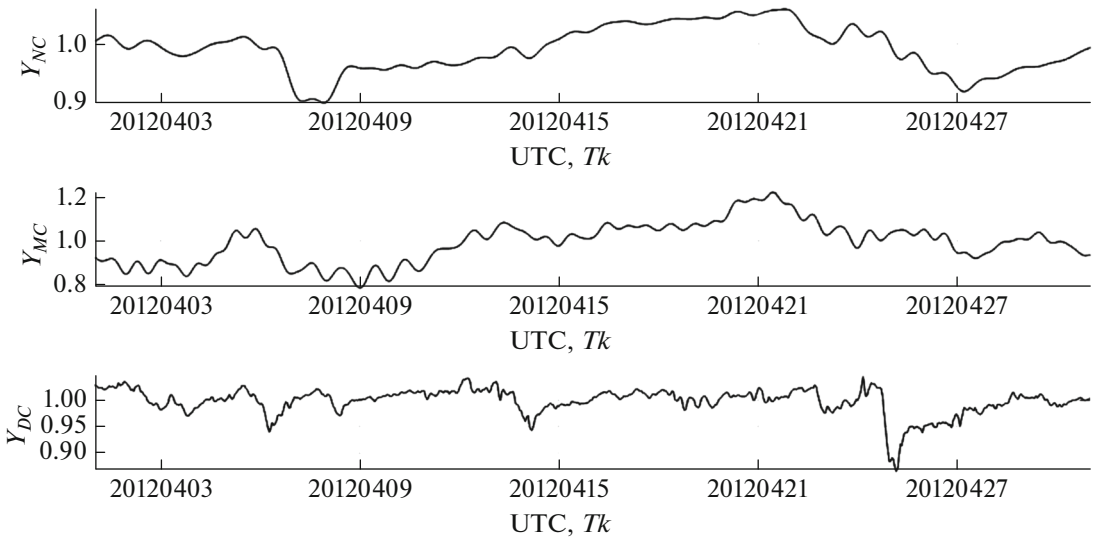

Fig. 3. Graphs of the variables $Y_{MP}(k)$, $Y_{NP}(k)$, and $Y_{DP}(k)$ derived from the numerical preprocessing on the monthly interval.

model *Dst* indices on the basis of NN models in the interval with the indices $k_{f0} + 1 \le k \le k_f$. For testing, an extrapolation algorithm over the variables $Y_{MC2}(k)$ and $Y_{NC2}(k)$ is implemented in order to further use the extrapolations in the generated NN models.

Figure 4 shows examples of the plots of variables $Y_{MC} = Y_{MC2}(k)$, $Y_{NC} = Y_{NC2}(k)$ obtained by filtering and scaling on the 4-day interval of April 1, 2012—April 4, 2012, and prepared for extrapolation. It can be concluded that the variables $Y_{MC2}(k)$, $Y_{NC2}(k)$ are well suited for extrapolation: it can be seen that their successful extrapolation based on parabolic functions is quite acceptable at least for $k_e = 5$–10 steps ahead.

4.2. Extrapolation formulas are implemented based on approximation parabolic models with respect to the current index k; the extrapolation parameter k_e, the number of extrapolation steps $k + 1, k + 2, ..., k + k_e$, is set. The number of indices in the interval $k, k - 1, ..., k - k_a + 1$, in which the approximation model is supposed to be built, is set. Parabolic approximation functions with parameters $c_1^T = (c_{01}, c_{11}, c_{21})$, $c_2^T = (c_{02}, c_{12}, c_{22})$ and approximation functionals are formed

$$F(c_1, Y_{MC2}, k_a, k) = \sum_{s=k-k_a+1}^{k} (Y_{MC2}(s) - c_{01} - c_{11}s - c_{21}s^2)^2,$$

$$F(c_2, Y_{NC2}, k_a, k) = \sum_{s=k-k_a+1}^{k} (Y_{NC2}(s) - c_{02} - c_{12}s - c_{22}s^2)^2.$$

Optimal parameters of the approximation models are determined by minimizing the introduced functionals

$$c_1^\circ = \arg\{\min_{c_1} F(c_1, Y_{MP2}, k_a, k)\},$$

$$c_2^\circ = \arg\{\min_{c_2} F(c_2, Y_{NP2}, k_a, k)\}.$$

The extrapolated models $\bar{Y}_{MC2} = \bar{Y}_{MC2}(k, k_e)$, $\bar{Y}_{NC2} = \bar{Y}_{NC2}(k, k_e)$ are formed on Δk-dimension intervals moving in unit steps. For k_e indices $k + 1, k + 2, ..., k + k_e$, the extrapolated models are represented by the parabolic approximation functions

$$\begin{aligned} \bar{Y}_{MC2}(k, k_e) &= c_{01}^\circ + c_{11}^\circ k + c_{21}^\circ k^2, \\ \bar{Y}_{NC2}(k, k_e) &= c_{02}^\circ + c_{12}^\circ k + c_{22}^\circ k^2. \end{aligned} \quad (1)$$

For $\Delta k - k_e$ indices $k + k_e - \Delta k + 1$, $k + k_e - \Delta k + 2, ..., k$, the extrapolated models are represented by formulas

$$\begin{aligned} \bar{Y}_{MC2}(k, k_e) &= \bar{Y}_{MC2}(k), \\ \bar{Y}_{NC2}(k, k_e) &= \bar{Y}_{NC2}(k). \end{aligned} \quad (2)$$

Moving extrapolated model estimates of *Dst* indices are computed using NN models for the extrapolated MH, NM observations $\bar{Y}_{DM} = \bar{Y}_{MC2}(k, k_e)$, $\bar{Y}_{DN} = \bar{Y}_{NC2}(k, k_e)$ in the interval $k_{1T} \le k \le k_{2T}$. In order to calculate k_{1T}, k_{2T}, the following inequalities derived from (1)–(2) are written

$$k_{f0} + 1 \le k + k_e - \Delta k + 1, \quad k + k_e \le k_f.$$

The solution of these inequalities makes it possible to determine the boundary indices

$$k_{1T} = k_{f0} - k_e + \Delta k, \quad k_{2T} = k_f - k_e. \quad (3)$$

The decision rule algorithm for predicting GMS's is based on the computed moving extrapolated model estimates of *Dst* indices $\bar{Y}_{DM}$, $\bar{Y}_{DN}$ and comparing them

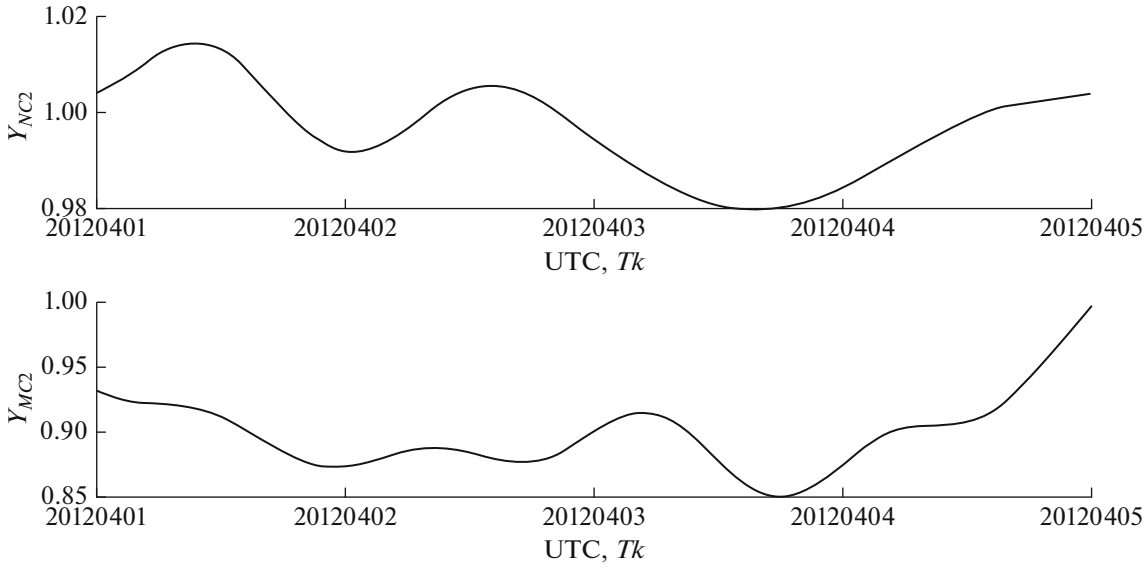

Fig. 4. Graphs of variables $Y_{MP2}(k)$, $Y_{NP2}(k)$ obtained from filtering and scaling operations on the 4-day interval (Apr. 1–Apr. 4, 2012).

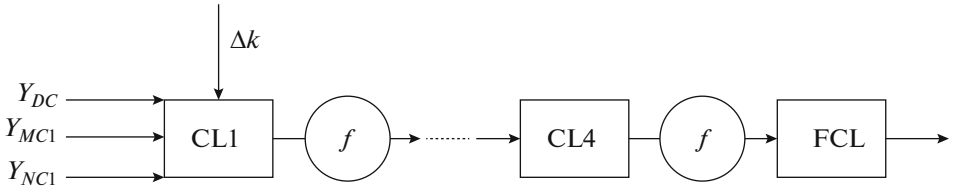

Fig. 5. NN architecture.

to a given threshold Y_{D0}. GMS prediction decision making is implemented in the interval $k_{1T} \le k \le k_{2T}$ (3).

5. NN ARCHITECTURE

The results obtained above are based on a fully-connected feed-forward NN generated using a generic software product (Deep Learning, 2021). The use of NN of this type is due to the fact that in this case the raw data and observations are scalar time series.

The architecture of the used NN is presented in Fig. 5. Four connected layers (CLs) with input variables Y_{DC}, Y_{MC1}, Y_{NC1} were implemented, on the basis of which the Δk-dimension input vector sequences were formed. Activation functions $f(x) = 1, x > 0, f(x) = 0, x \le 0$ were used. The outputs from the four layers C$L1$–C$L4$ were fed to the summing fully-connected layer (FCL). The NN output at the training stage is the generated NN models.

The indices of the intervals of initial variables took numerical values in accordance with item 2 and were assigned $dk_{01} = 12000$, $dk_{02} = 15000$. The index $k_{f0} = 131810$ corresponding to the date of January 1, 2017, was assigned, which defined the 8-year training interval (January 1, 2008–December 31, 2016) for the MH and the 14-year interval (January 1, 2002–December 31, 2016) for the NM. The 2-year interval (January 1, 2017–December 31, 2018) was allotted to compute model estimates of *Dst* indices based on MH, NM observations using NN model structures.

6. THE GMS PREDICTION DECISION RULE

We reduce the GMS prediction method to a classification procedure (Bishop, 2006; Fomin, 2010) based on comparing extrapolated model estimates of *Dst* indices to a given threshold for the current index k given the extrapolation steps k_e.

We create a decision rule for GMS prediction decisions based on the joint use of MH, NM model estimates of *Dst* indices, which is that if at least one or both conditions for the current index k are met

$$\bar{Y}_{DM}(k, k_e) \le Y_{D0} \quad \text{and/or} \quad \bar{Y}_{DN}(k, k_e) \le Y_{D0}, \quad k_{1T} \le k \le k_{2T}, \tag{4}$$

then we will make a GMS prediction decision for the index $k + k_e$; in other cases, we will make the opposite decision.

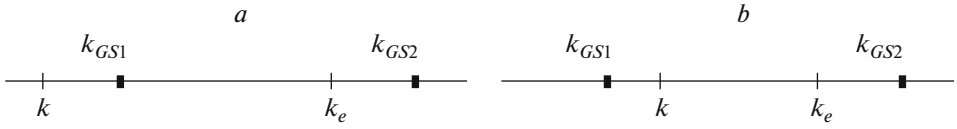

Fig. 6. First and second variants of GMS predictions.

Let us provide clarifications on the implementation of the prediction. We assume that the possible GMS was implemented on a time interval with indices that satisfied the inequalities $k_{GS1} \le k \le k_{GS2}$. We will still assume that the prediction is performed for a point in time with the index k for k_e indices forward. We consider two possible cases: 1. When the time k of making a prediction is outside the interval with the GMS; 2. When the time k of making a prediction is inside the interval with the GMS. In that case, even if both prediction variants are implemented, which is equivalent to the inequality $k_{GS1} \le k_e \le k_{GS2}$, the variants are significantly different. For the first variant, the implemented variant is quite complete, because the prediction was implemented in advance with respect to the GMS. In the second variant, the prediction took place when the GMS had already occurred. Figures 6a and 6b show the predictions for the first and second variants. The following inequalities correspond to the first and second variants of the GMS prediction

$$k \le k_{GS1} \le k_e \le k_{GS2}, \quad k_{GS1} \le k < k_e \le k_{GS2},$$

7. CALCULATING ESTIMATES OF THE PROBABILITIES OF CORRECT AND FALSE GMS PREDICTIONS

GMS prediction is usually accompanied by errors, such as incorrect forecasting and generation of false predictions. These errors depend on the probability characteristics of the variables $\bar{Y}_{DM}$, $\bar{Y}_{DN}$. Let us use the results of (Merkov, 2014; Mikhailov and Voitishek, 2006) for their approximate calculation. Let us form estimates of prediction error probabilities, in which we use the initial *Dst* indices $Y_D(k)$, model estimates of predicted *Dst* indices $\bar{Y}_{DM}(k, k_e)$, $\bar{Y}_{DN}(k, k_e)$, which are random. We implement calculations for a number of variants of extrapolation steps k_e and use decision rule (4).

We fix the threshold Y_{D0} and consider the time with the index $k + k_e$ in which GMS takes place if the inequality $Y_D(k + k_e) \le Y_{D0}$ is satisfied. We calculate the number N_{GS} of the states with the GMS which are determined by the fulfillment of this inequality in the interval $k_{1T} \le k \le k_{2T}$ using the following sum

$$N_{GS} = \sum_{k=k_{1T}}^{k_{2T}} \operatorname{sgn}(Y_{D0} - Y_D(k + k_e)), \tag{5}$$

where $\operatorname{sgn} x = 1, x \ge 0, \operatorname{sgn} x = 0, x < 0$. Let us determine $N_{M,GS}$, which is the number of correct GMS predictions using $\bar{Y}_{DM}(k, k_e)$ based on (4), and find β_M, which is an estimate of the probability of correct forecasting

$$N_{M,GS} = \sum_{k=k_{1T}}^{k_{2T}} \operatorname{sgn}(Y_{D0} - Y_D(k + k_e)) \times \operatorname{sgn}(Y_{D0} - \bar{Y}_{DM}(k, k_e)), \quad \beta_M^\circ = \frac{N_{M,GS}}{N_{GS}}. \tag{6}$$

We count the number $N_{N,GS}$ of correct GMS predictions using $\bar{Y}_{DN}(k, k_e)$ using (4) and determine an estimate of the probability of correct forecasting β_N

$$N_{N,GS} = \sum_{k=k_{1T}}^{k_{2T}} \operatorname{sgn}(Y_{D0} - Y_D(k + k_e)) \times \operatorname{sgn}(Y_{D0} - \bar{Y}_{DN}(k, k_e)), \quad \beta_N^\circ = \frac{N_{N,GS}}{N_{GS}}. \tag{7}$$

The estimate of the probability of correct GMS predictions β_{MN} when $\bar{Y}_{DM}(k, k_e)$, $\bar{Y}_{DN}(k, k_e)$ and (4) are used together is found as follows

$$N_{MN,GS} = \sum_{k=k_{1T}}^{k_{2T}} \operatorname{sgn}[Y_{D0} - Y_D(k + k_e)) \times \operatorname{sgn}(\operatorname{sgn}(Y_{D0} - \bar{Y}_{DN}(k, k_e)) + \operatorname{sgn}(Y_{D0} - \bar{Y}_{DM}(k, k_e))], \quad \beta_{MN}^\circ = \frac{N_{MN,GS}}{N_{GS}}. \tag{8}$$

The numbers N_{0GS}, $N_{M,0GS}$, $N_{N,0GS}$, $N_{MN,0GS}$ and the probabilities of false predictions of the GMS α_M°, α_N°, α_{MN}° will be calculated by formulas similar to (5)–(8). Calculations by formulas (5)–(8) are implemented for the set of extrapolation steps k_e. We determine the probabilities of omitting predictions for MH, NM, and MH|NM by the differences $1 - \beta_M^\circ$, $1 - \beta_N^\circ$, and $1 - \beta_{MN}^\circ$.

8. EXPERIMENTAL STUDY OF THE GMS PREDICTION METHOD

8.1. Estimating the Probability of Correct and False GMS Predictions Depending on the Extrapolation Step k_e

In an interval with indices $k_{1T} \le k \le k_{2T}$, the time series $Y_D(k)$ of *Dst* indices from the database (World Data Center, 2021) was examined. For the given inte-

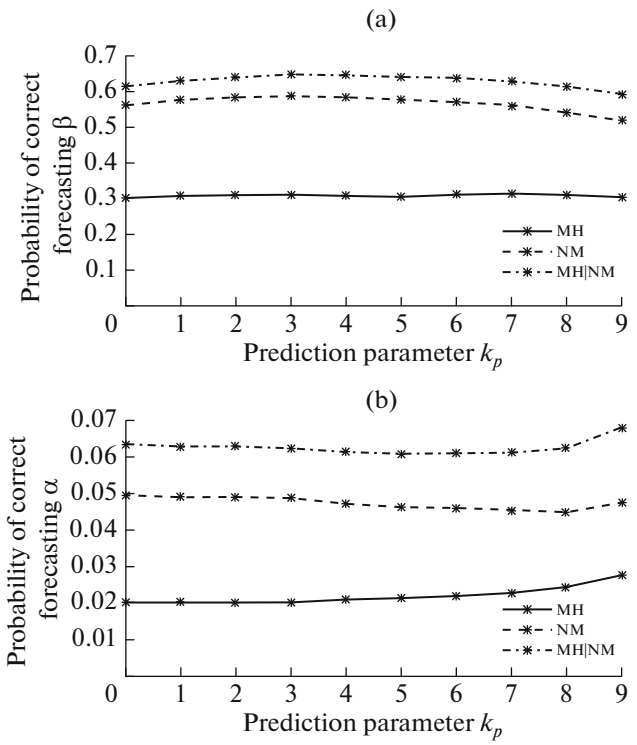

Fig. 7. (a) Estimates β°_{M}, β°_{N}, β°_{MN} of probabilities of correct GMS forecasting. (b) Estimates α°_{M}, α°_{N}, α°_{MN} of probabilities of false GMS forecasting.

ger parameters k_e, extrapolated model estimates $\bar{Y}_{DM}(k, k_e)$, $\bar{Y}_{DN}(k, k_e)$ were calculated and compared with the Y_{D0} threshold, and the probabilities of correct and false GMS predictions were determined using formulas (5)–(8) as a function of the parameter k_e for the range $k_{e,mn} \le k_e \le k_{e,mx}$, $k_{e,mn} = 0$, $k_{e,mx} = 9$ for $Y_{D0} = -50$ nT.

Figures 7a and 7b present graphs of the results of calculations of the estimates of probabilities of correct forecasting β°_{M}(MH), β°_{N}(NM), β°_{MN} (MH|NM) and probabilities of false prediction α°_{M}(MH), α°_{N}(NM), α°_{MN} (MH|NM) depending on k_e. From the presented graphs with the results of the calculations, it can be seen that the combined use of MH and NM observations increased the efficiency of GMS prediction. From Fig. 7a, we can conclude that for the prediction parameter $k_e = 5$, the probability of correct joint GMS prediction took the maximum value and was $\beta^{\circ}_{MN} \approx 0.65$, which is greater than the corresponding value $\beta^{\circ}_{N} \approx 0.57$ by 13–15%. The probability of false joint prediction, according to Fig. 7b, did not exceed $\alpha^{\circ}_{MN} \approx 0.06$.

8.2. Calculating GMS Predictions for a Given Time Interval

An initial time interval with indices $k_{1T} \le k \le k_{2T}$ was considered, on which model estimates of *Dst* indices were computed and the GMS prediction problem was solved. In this interval, the time series $Y_D(k)$ was formed and extrapolated model estimates $\bar{Y}_{DM}(k, k_e)$, $\bar{Y}_{DN}(k, k_e)$ were calculated for the given values of the extrapolation parameter k_e.

The control interval with indices k_{1C}, k_{2C} that satisfied the inequalities $k_{1T} < k_{1C} \le k \le k_{2C} < k_{2T}$ was considered. Sequences of intervals $k_{GS1} \le k \le k_{GS2}$ in which GMS occurred were determined by checking inequalities for moving k and the given value of the extrapolation parameter k_e

Table 1. Extrapolation $k_e = 5$, 2017

N_0	Tk_{GS1}	Tk_{GS2}	Tk_{M1}	Tk_{M2}	Tdk_M	Tk_{N1}	Tk_{N2}	Tdk_N	Tdk_e
1	05.28.00	05.28.20	–	–	–	05.27.21	05.29.11	+3	+3–cf
2	07.16.12	07.17.17	07.16.21	07.17.17	–5	07.16.08	07.17. 21	+4	+4–cf
3	09.07.23	09.10.03	09.08.03	09.08.21	–4	09.07.21	09.10.09	+2	+2–cf
4	09.14.20	09.14.21	–	–	–	09.14.15	09.15.17	+5	+5–cf
5	09.28.01	09.28.13	–	–	–	–	–	–	–mcf

Table 2. Extrapolation $k_e = 7$, 2015

N_0	Tk_{GS1}	Tk_{GS2}	Tk_{M1}	Tk_{M2}	Tdk_M	Tk_{N1}	Tk_{N2}	Tdk_N	Tdk_e
1	08.25.23	08.26.09	08.26.09	08.27.11	–10	08.25.22	08.26.14	+1	+1–cf
2	09.10.18	09.11.20	–	–	–	09.10.11	09.10.21	+7	+7–cf
3	09.22.02	09.22.20	09.22.11	09.22.12	–9	–	–	–9	–9–mcf
4						10.07.18	10.08.12		ff

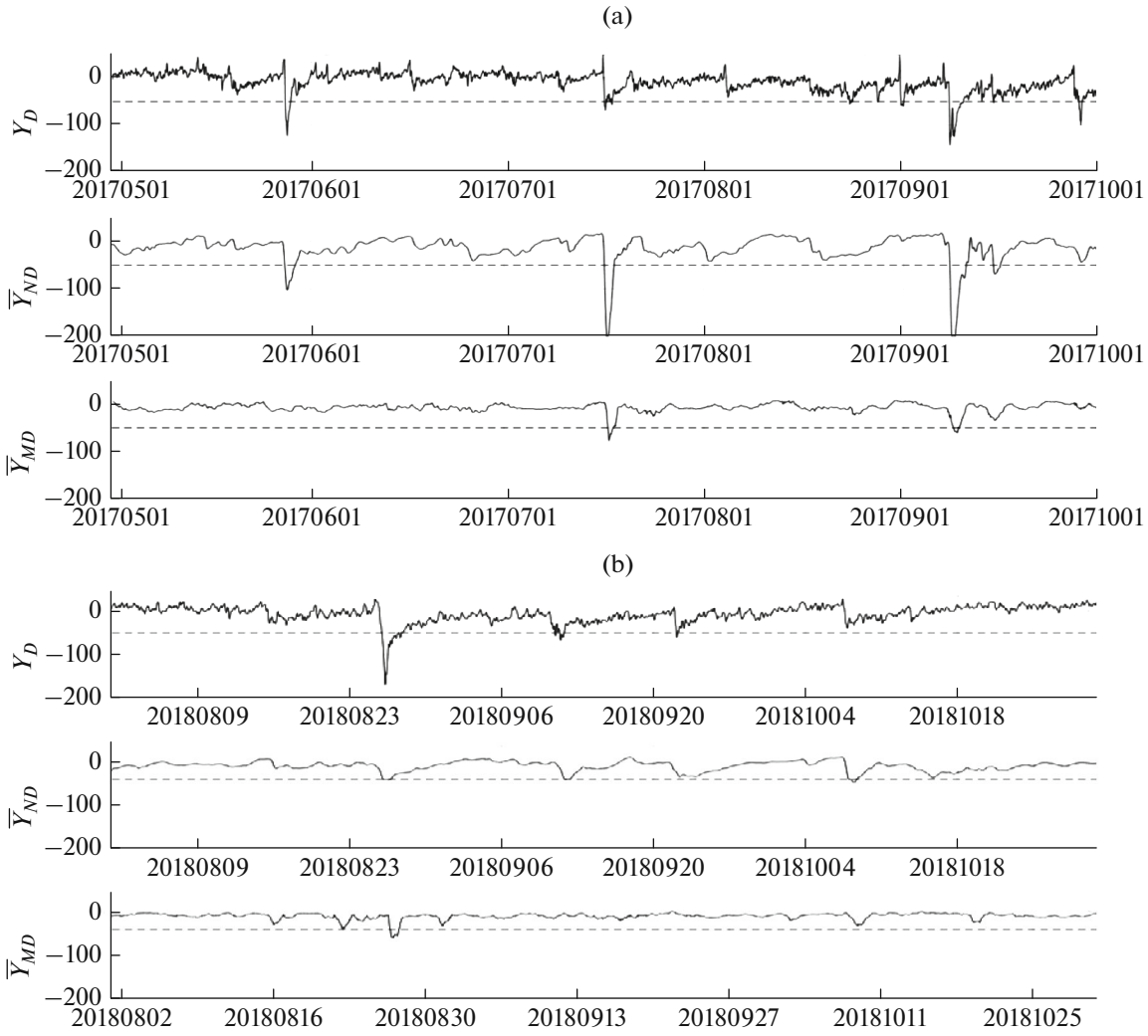

Fig. 8. (a) Graphs of the variables $Y_D(k)$, $\bar{Y}_{DM}(k, k_e)$, and $\bar{Y}_{DN}(k, k_e)$, $k_e = 5$. (b) Graphs of the variables $Y_D(k)$, $\bar{Y}_{DM}(k, k_e)$, and $\bar{Y}_{DN}(k, k_e)$, $k_e = 7$.

$$Y_D(k + k_e) \le Y_{D0}, \quad k_{1C} \le k \le k_{2C}.$$

Sequences of intervals $k_{M1} \le k \le k_{M2}$ and $k_{N1} \le k \le k_{N2}$, in which GMS predictions were made according to decision rule (4), were determined by checking the following inequalities

$$\bar{Y}_{DM}(k, k_e) \le Y_{D0}, \quad \bar{Y}_{DN}(k, k_e) \le Y_{D0}.$$

The GMS predictions took into account the mutual arrangement of intervals (k_{GS1}, k_{GS2}) and (k_{M1}, k_{M2}), (k_{N1}, k_{N2}). Time differences Tdk_M, Tdk_N for separate observations and differences Tdk_{MN}, where $k_{MN} = \max(k_{M1}, k_{N1})$ for joint MH, NM observations were introduced to assess the effectiveness of GMS predictions

$$Tdk_M = Tk_{GS1} - Tk_{M1}, \quad Tdk_N = Tk_{GS1} - Tk_{N1},$$
$$Tdk_{MN} = Tk_{GS1} - Tk_{MN}.$$

Obviously, GMS predictions make sense when the inequalities $Tdk_M > 0$, $Tdk_N > 0$, and $Tdk_{MN} > 0$ were satisfied in separate and joint observations.

Depending on the positions (k_{GS1}, k_{GS2}) and (k_{M1}, k_{M2}), (k_{N1}, k_{N2}), there are obviously possible implementations of correct forecasting (cf), miss of correct forecasting (mcf), and false forecasting (ff) of GMS's. The larger the values of the introduced differences, the more advance the GMS prediction is. Negative values for dk_M, dk_N, dk_{MN} can be assumed to correspond to missing forecasts, mfc.

For the first example, a reference time interval of 5 months (May 1, 2017–September 30, 2017) was considered; $Y_D = Y_D(k)$ and $\bar{Y}_{DM} = \bar{Y}_{DM}(k, k_e)$, $\bar{Y}_{DN} = \bar{Y}_{DN}(k, k_e)$ with $k_e = 5$ were used. Figure 8a shows graphs for these variables. The dotted line indicates the assigned threshold $Y_{D0} = -52.5$ nT. The results of the prediction calculations are presented in Table 1;

for space considerations, the year 2017 is omitted from the dates; the columns contain the calendar variables, such as month, day, and hour, derived from the conversion of the k indices. Columns 2, 3 contain times of the intervals (Tk_{GS1}, Tk_{GS2}) of start and end of the events due to $Y_D(k)$ reductions, which can turn out to be GMS events; the first column defined numbers N_0 of intervals with GMS events. Columns 4, 5 and 7, 8 contain interval times (Tk_{M1}, Tk_{M2}), (Tk_{N1}, Tk_{N2}) with 1-hour accuracy. A total of 5 GMS events took place. From the contents of column 10 with prediction time $Tdk_e = \max(Tdk_M, Tdk_N)$, we can conclude that correct GMS predictions were made in four events, $N_{cf} = 4$: for no. 1, prediction was made in 3 h, no. 2, in 4 h, no. 3, in 2 h, and 4, in 5 h. For event no. 5, there was a miss of correct forecasting $N_{mf} = 1$. There were 0 false forecasts, $N_{ff} = 0$.

For the second example, the 3-month reference interval (August 1, 2015–October 31, 2015) was considered and $Y_D = Y_D(k)$ and $\bar{Y}_{DM} = \bar{Y}_{DM}(k, k_e)$, $\bar{Y}_{DN} = \bar{Y}_{DN}(k, k_e)$ with $k_e = 7$ were used; the threshold $Y_{D0} = -52.5$ nT was assigned. Figure 8b shows the corresponding graphs of the variables with the dotted line indicating the threshold. The results of the calculations are presented in Table 2. Three GMS-events took place during the 3-month interval under consideration. We can conclude from the contents of column 10 that correct GMS predictions were made in two cases, $N_{cf} = 2$: for no. 1, prediction was made in 1 h and for no. 2, in 7 h. There was one false forecast, $N_{ff} = 1$, and one miss of correct forecasting, $N_{mf} = 1$.

In order to approximate the effectiveness of the GMS prediction method, we introduced coefficients of correct and false forecasting ε_{cf} and ε_{ff}, whose quite obvious physical meaning is derived from the following formulas

$$\varepsilon_{cf} = N_{cf}/(N_{cf} + N_{mf}), \quad \varepsilon_{ff} = N_{ff}/N_{cf}.$$

The calculation of the coefficients on the basis of Tables 1 and 2 allowed us to establish their average values $\bar{\varepsilon}_{cf} \approx 73\%$, $\bar{\varepsilon}_{mf} \approx 25\%$, which can be taken as first approximations of estimates of the effectiveness of the proposed prediction method.

9. CONCLUSIONS

1. The proposed method for predicting geomagnetic storms (GMS) on the basis of joint observations of the URAGAN muon hodoscope and neutron monitors using a fully-connected feed-forward NN and extrapolated model estimates of *Dst* indices is operational.

2. The study of the proposed method of GMS prediction on observations of the muon hodoscope, neutron monitors, and *Dst* indices obtained for 2008–2018 and 2002–2018 showed its effectiveness.

3. The conducted calculations of the combined use of MN and NM observations showed that for the optimal prediction parameter $k_e = 5$, the estimated probability of correct GMS prediction is $\beta^{\circ}_{MN} \approx 0.65$, which is greater than the corresponding value $\beta^{\circ}_{N} \approx 0.57$ by 13–15%; the probability of false forecasting does not exceed $\alpha^{\circ}_{MN} \approx 0.06$.

4. The consideration of examples of experimental data on 5-month intervals showed that it is possible to implement the coefficients of correct and false forecasting ≈73%, ≈25% using the proposed method, which indicates acceptable capabilities of the proposed method.

5. The proposed GMS prediction method has a lot of room for improvement, in particular, in terms of further optimization of the NN parameter settings in order to increase correct prediction probabilities and decrease false prediction probabilities.

6. The proposed GMS prediction method has a favorable outlook for its use in applied geophysical problems.

ACKNOWLEDGMENTS

We thank A.V. Belov (Candidate of Physical and Mathematical Sciences), V.G. Yanke (Candidate of Physical and Mathematical Sciences), and A.A. Abunina (IZMIRAN) for the given possibility to use specially prepared NM observations and useful comments during the preparation of the manuscript.

FUNDING

This work was carried out within the State Task of the Geophysical Center of the Russian Academy of Sciences approved by the Ministry of Science and Higher Education of the Russian Federation.

CONFLICT OF INTEREST

The authors declare that they have no conflicts of interest.

REFERENCES

Abunina, M.A., Abunin, A.A., Belov, A.V., Eroshenko, E.A., Oleneva, V.A., and Yanke, V.G., Global survey method for the world network of neutron monitors, *Geomagn. Aeron. (Engl. Transl.)*, 2018, vol. 58, no. 3, pp. 356–372. https://doi.org/10.1134/S0016793218030039

Barkhatov, N.A. and Revunov, S.E., *Iskusstvennye neironnye seti v zadachakh solnechno–zemnoi fiziki* (Artificial Neural Networks in Problems of Solar–Terrestrial Physics), Nizhny Novgorod: Povolzh'e, 2010.

Barkhatov, N.A., Korolev, A.V., Ponomarev, S.M., and Sakharov, S.Yu., Long-term forecasting of solar activity indices using neural networks, *Radiophys. Quantum Electron.*, 2001, vol. 44, no. 9, pp. 742–749.

Bishop, C.M., *Pattern Recognition and Machine Learning*, New York: Springer, 2006.

Borog, V.V., *Osnovy myuonnoi diagnostiki* (Fundamentals of Muon Diagnostics), Moscow: MIFI, 2008.

Chinkin, V.E., Astapov, I.I., Gvishiani, A.D., Getmanov, V.G., Dmitrieva, A.N., Dobrovolsky, M.N., Kovylyaeva, A.A., Sidorov, R.V., Soloviev, A.A., and Yashin, I.I., Method for the identification of heliospheric anomalies based on the functions of the characteristic deviations for the observation matrices of the muon hodoscope, *Phys. Atom. Nuclei*, 2019, vol. 82, pp. 924–928. https://doi.org/10.1134/S106377881966013X

Deep Learning Toolbox—MATLAB, 2021. https://www.mathworks.com/products/deep-learning.html.

Dobrovolsky, M.N., Astapov, I.I., Barbashina, N.S., et al., A way of detecting local muon-flux anisotropies with the matrix-form data of the URAGAN hodoscope, *Bull. Russ. Acad. Sci.: Phys.*, 2019, vol. 83, no. 5, pp. 647–649. https://doi.org/10.3103/S1062873819050125

Dolenko, S.A., Orlov, Y.V., Persiantsev, I.G., and Shugai, J.S., Neural network algorithm for events forecasting and its application to space physics data, in *Artificial Neural Networks: Formal Models and Their Applications, ICANN-2005*, Duch, W., Kacprzyk, J., Oja, E., and Zadrożny S., Eds., Berlin: Springer, 2005, pp. 527–532. https://doi.org/10.1007/11550907_83

Efitorov, A.O., Myagkova, I.N., Shirokii, V.R., and Dolenko, S.A., The prediction of the *Dst*-index based on machine learning methods, *Cosmic Res.*, 2018, vol. 56, no. 6, pp. 434–441. https://doi.org/10.1134/S0010952518060035

Filter Design Using MATLAB, 2021. https://www.mathworks.com/discovery/filter-design.html.

Fomin, Ya.A., *Raspoznavanie obrazov: teoriya i primeneniya* (Pattern Recognition: Theory and Experiment), Moscow: Fazis, 2010.

Gaidash, S.P., Belov, A.V., Abunin, A.A., and Abunina, M.A., The IZMIRAN space weather forecast center, in *Sbornik dokladov 11-oi ezhegodnoi konferentsii "Fizika plazmy v solnechnoi sisteme", Materialy spetsial'noi sektsii "Prakticheskie aspekty nauki kosmicheskoi pogody"* (Proceedings of the 11th Annual Conference "Plasma Physics in the Solar System", Special Section: Practical Aspects of Space Weather Science), Petrukovich, A.A., Merzlyi, A.M., and Khabibulin, S.Yu., Eds., Moscow: IKI RAN, 2016, pp. 22–32.

Gaidash, S.P., Belov, A.V., Abunina, M.A., and Abunin, A.A., Space weather forecasting at IZMIRAN, *Geomagn. Aeron. (Engl. Transl.)*, 2017, vol. 57, pp. 869–876. https://doi.org/10.1134/S0016793217070088

Gruet, M.A., Chandorkar, M., Sicard, A., and Camporeale, E., Multiple-hour-ahead forecast of the *Dst* index using a combination of long short-term memory neural network and Gaussian process, *Space Weather*, 2018, vol. 16, no. 11, pp. 1882–1896. https://doi.org/10.1029/2018SW001898

Laboratory of solar X-ray astronomy, Lebedev Physical Institute of the Russian Academy of Sciences, 2021. https://tesis.lebedev.ru/.

Menvielle, M., Iyemori, T., Marchaudon, A., and Nose, M., Geomagnetic indices, in *Geomagnetic Observations and Models, IAGA Special Sopron Book Series 5*, Mandea, M. and Korte, M., Eds., Dordrecht: Springer, 2011, pp. 183–228. https://doi.org/10.1007/978-90-481-9858-0_8.

Merkov, A.B., *Raspoznavanie obrazov: Postroenie i obuchenie veroyatnostnykh modelei* (Pattern Recognition: Construction and Learning of Probabilistic Models), Moscow: URSS, 2014.

Mikhailov, G.A. and Voitishek, A.V., *Chislennoe statisticheskoe modelirovanie. Metody Monte-Karlo* (Numerical Statistical Modeling. Monte-Carlo Methods), Moscow: Akademiya, 2006.

NMDB: The Neutron Monitor Database, 2021. https://www.nmdb.eu/.

NOAA/NWS Space Weather Prediction Center, 2021. https://www.swpc.noaa.gov/.

Pallocchia, G., Amata, E., Consolini, G., Marcucci, M.F., and Bertello, I., Geomagnetic *Dst* index forecast based on IMF data only, *Ann. Geophys.*, 2006, vol. 24, pp. 989–999. https://doi.org/10.5194/angeo-24-989-2006

Real-time URAGAN data, 2015. http://nevod.mephi.ru/uragan_data.htm.

Shirokii, V.R., Comparison of neural network models for predicting the Dst geomagnetic index on different datasets and comparison of model quality assessment methods, in *XVII Vserossiiskaya nauchno-tekhnicheskaya konf. "Neiroinformatika-2015. Sbornik nauchnykh trudov"* (Proceedings of the XVII All-Russian Scientific and Technical Conference "Neuroinformatics-2015"), Moscow: NIYaU MIFI, 2015, vol. 2, pp. 51–60.

Space Weather Prediction Center of IZMIRAN, 2016. http://spaceweather.izmiran.ru/.

Stepanova, M.V. and Pérez, P., Autoprediction of *Dst* index using neural network techniques and relationship to the auroral geomagnetic indices, *Geofis. Int.*, 2000, vol. 39, no. 1, pp. 143–146. https://doi.org/10.22201/igeof.00167169p.2000.39.1.310

Sugiura, M. and Kamei, T., *Equatorial Dst Index, 1957–1986*, IAGA Bulletin no. 40, Saint-Maur-des-Fossés: ISGI Publications Office, 1991.

World Data Center for Geomagnetism, Kyoto, 2021. http://wdc.kugi.kyoto-u.ac.jp.

Wu, J.-G. and Lundstedt, H., Geomagnetic storm predictions from solar wind data with the use of dynamic neural networks, *J. Geophys. Res.*, 1997, vol. 102, no. A7, pp. 14255–14268. https://doi.org/10.1029/97JA00975

Yashin, I.I., Astapov, I.I., Barbashina, N.S., et al., Real-time data of muon hodoscope URAGAN, *Adv. Space Res.*, 2015, vol. 56, no. 12, pp. 2693–2705. https://doi.org/10.1016/j.asr.2015.06.003

Translated by O. Pismenov